Image removed due to copyright restrictions.

Please see: Fig. 1.3 in Maekawa, Sadamichi, and Teruya Shinjo. *Spin Dependent Transport in Magnetic Nanostructures.*

Figure 1.3: Resistivity vs temperature of pure Ni metal. T_c indicates the Curie temperature. The dotted curve is an extension of the resistivity curve in the paramagnetic region to the ferromagnetic region for comparison.

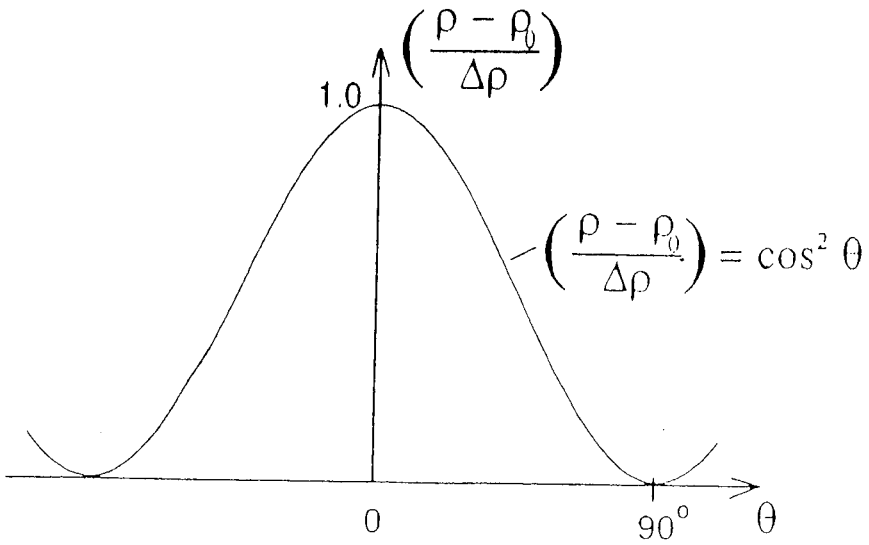

Fig.2 Graph of fractional magnetoresistive change versus θ according to equation (1).

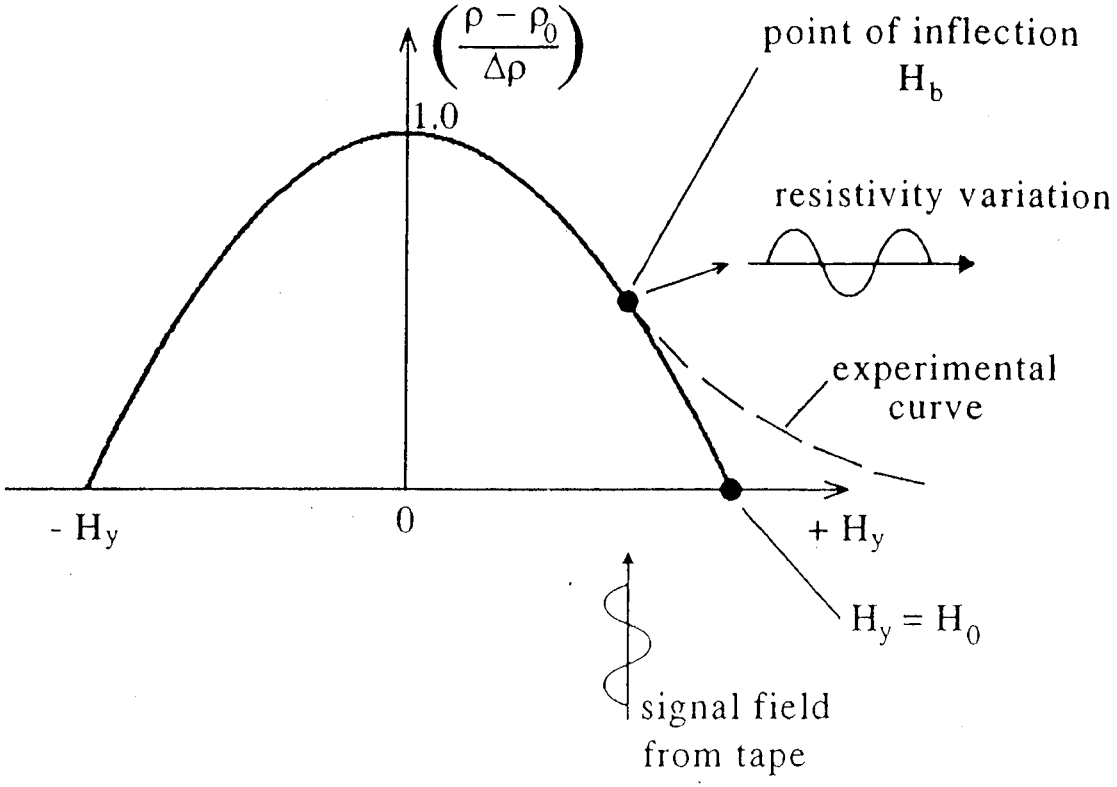

g.3 Graph of fractional magnetoresistive change versus transverse field H_y according to equation (7).

FIG 2

Images removed due to copyright restrictions.

Please see: Fig. 15.15 and 15.16 in O'Handley, Robert C. *Modern Magnetic Materials: Principles and Applications.*

Figure 15.16 Composition dependence of anisotropic magnetoresistance at room temperature. Left, Ni_xFe_{1-x} [after Bozorth (1946)]. Right, Ni_xCo_{1-x}, [after Smit (1951) and van Elst (1959)].

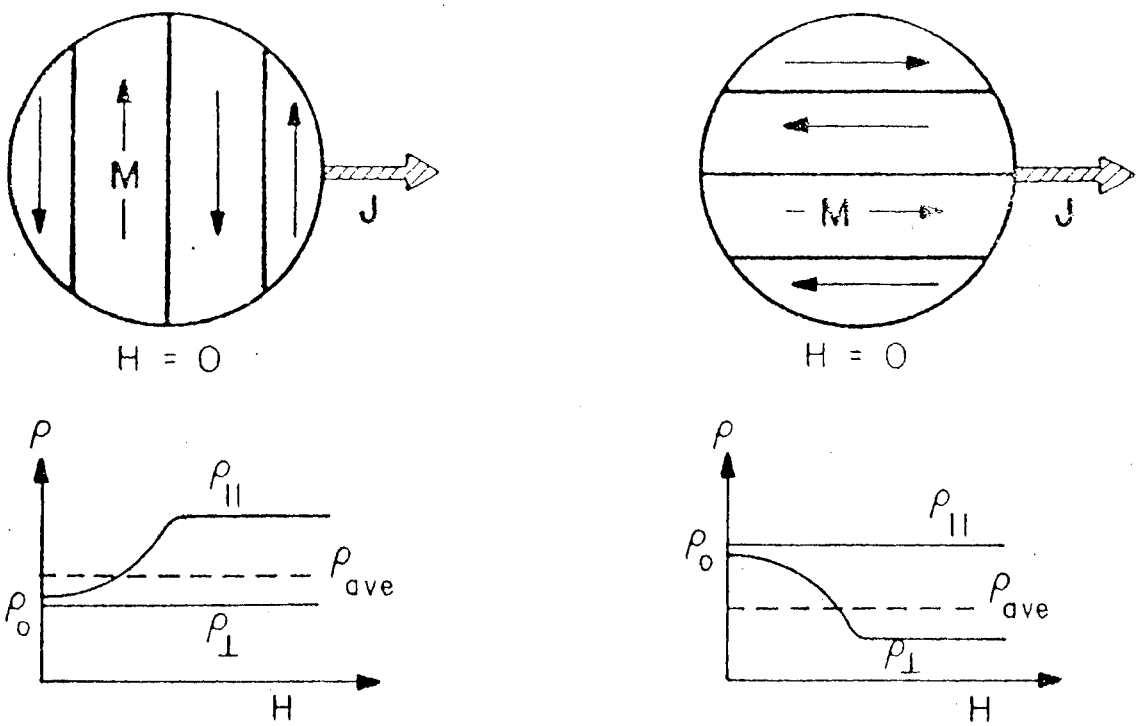

Figure 15.15 Field dependence of resistivity in fields parallel and perpendicular to J reveals the extraordinary or anisotropic magnetoresistance effect $\Delta\rho = \rho_{\parallel} - \rho_{\perp}$ at low fields superimposed on the ordinary effects (quadratic in H) at higher fields. Note that in zero field, the resistance may be larger or smaller than ρ_{av} depending on the equilibrium domain structure.

. APPLICATION IN MAGNETIC RECORDING

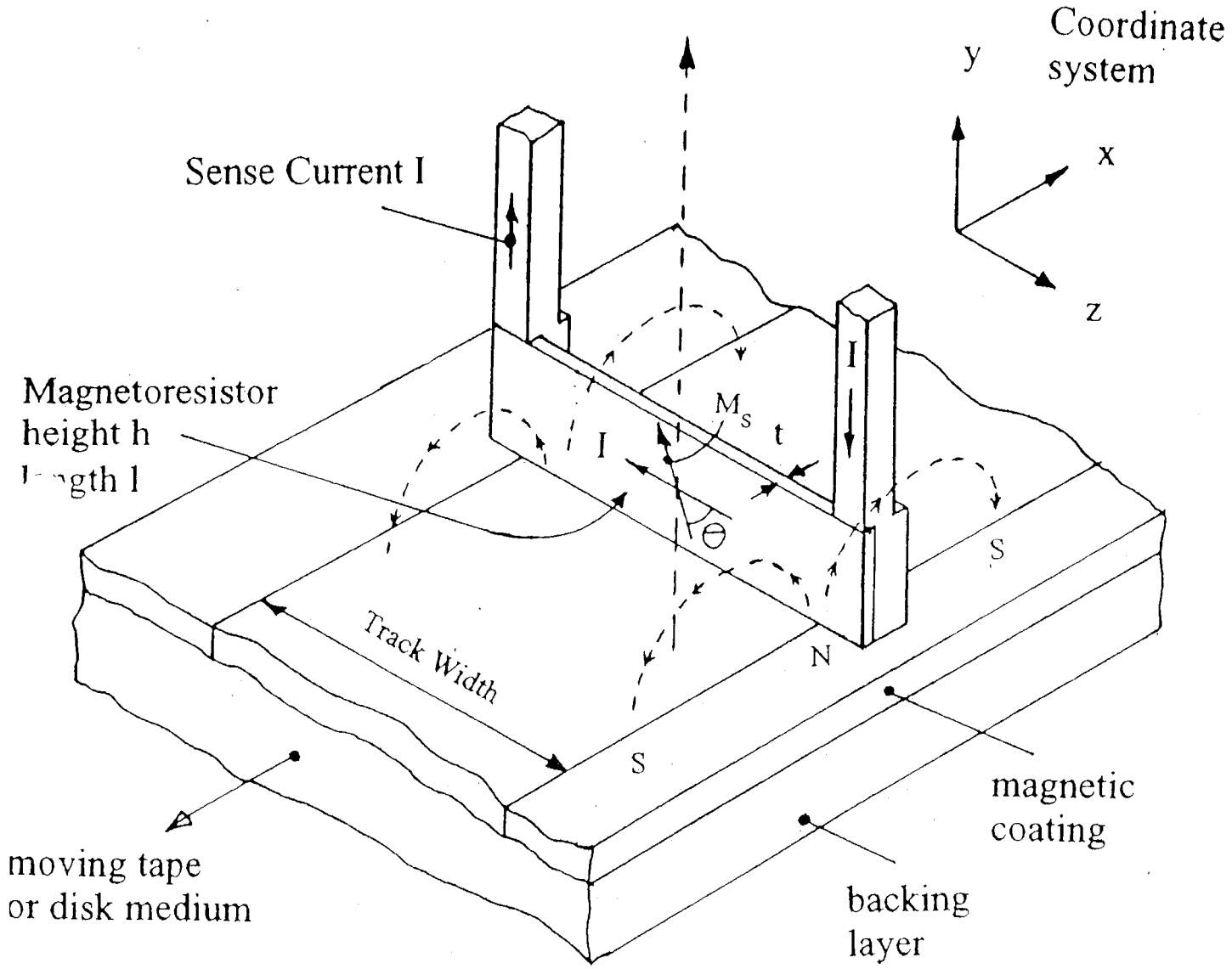

Playback using the magnetoresistance (MR) effect.

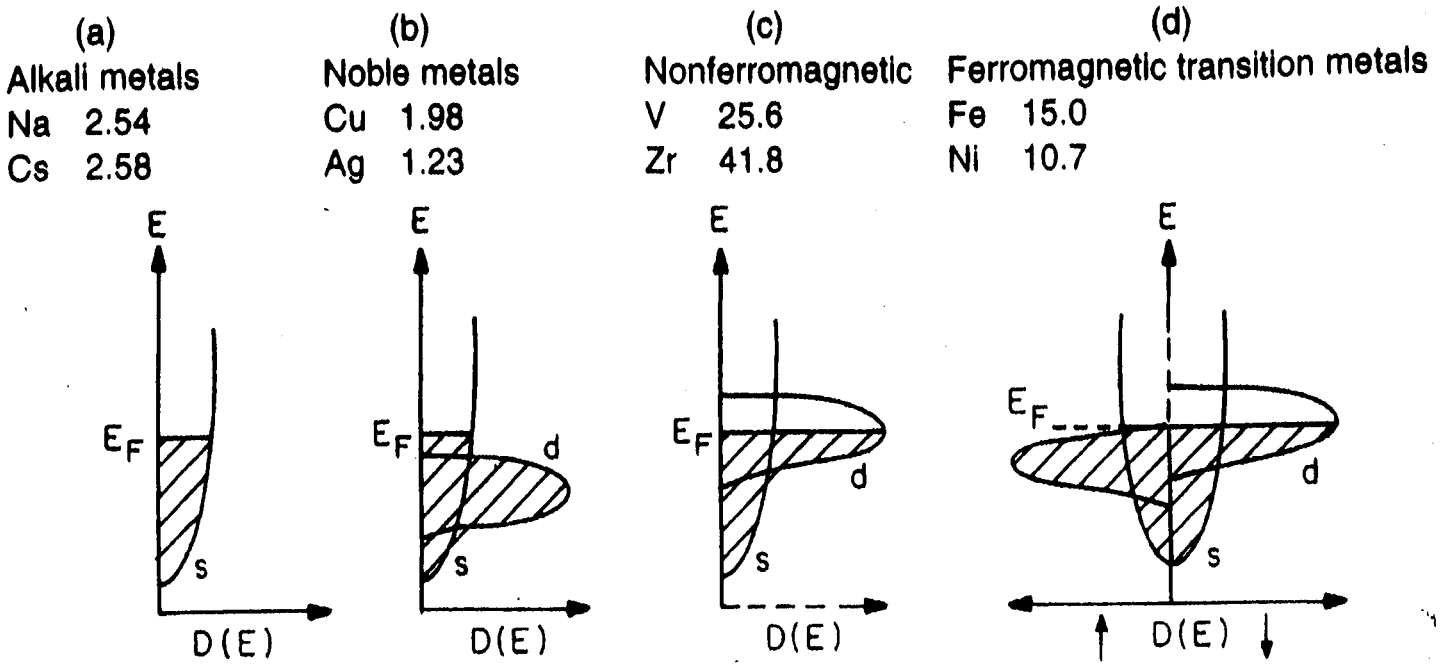

Figure 15.4 Examples of electrical resistivity at the Debye temperature (ρ in $\mu\Omega \cdot$ cm) for four classes of metals (below, schematic state densities for each class: (*a*) alkali metals; (*b*) noble metals; (*c*) nonferromagnetic transition metals; (*d*) ferromagnetic transition metals.

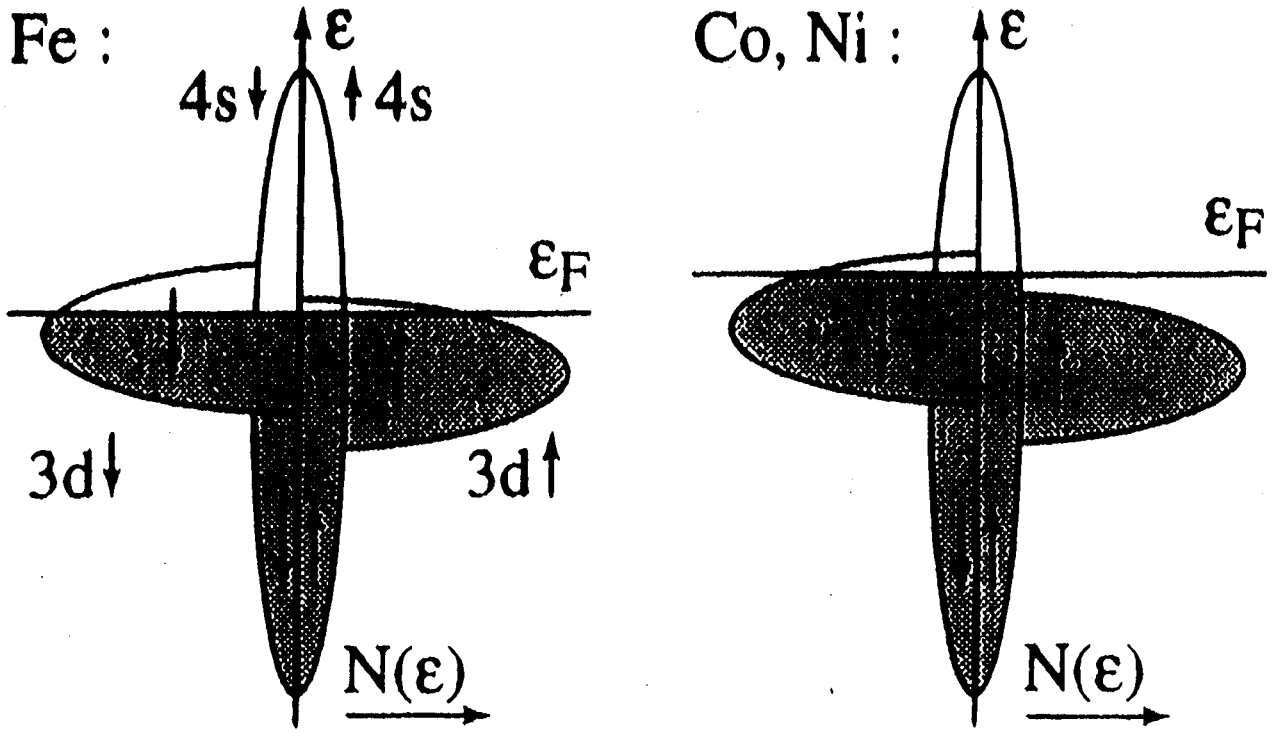

Figure 20.12 - Schematic representation of the band structures of the ferromagnetic transition metals (Fe, Co, Ni)

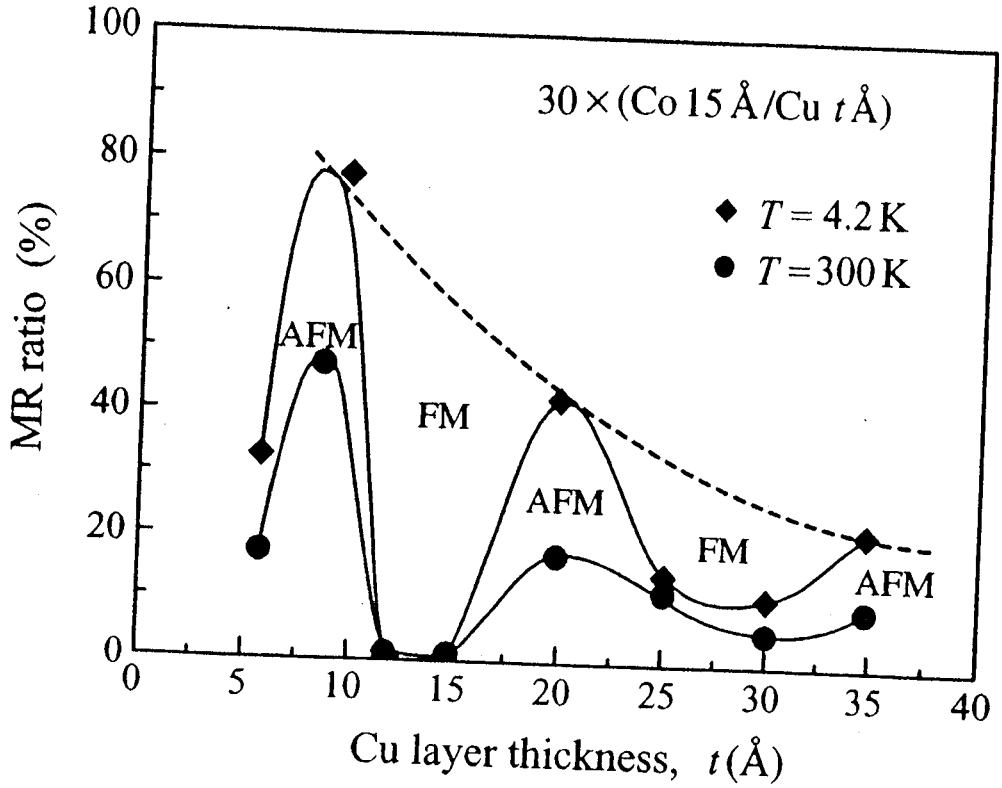

Figure 1.5: MR ratio of Cu/Co multilayers as a function of Cu layer thickne:

POSITIONS SAME FOR Co/Ni and Co/Fe or Co/$Fe_{20}Ni_{80}$

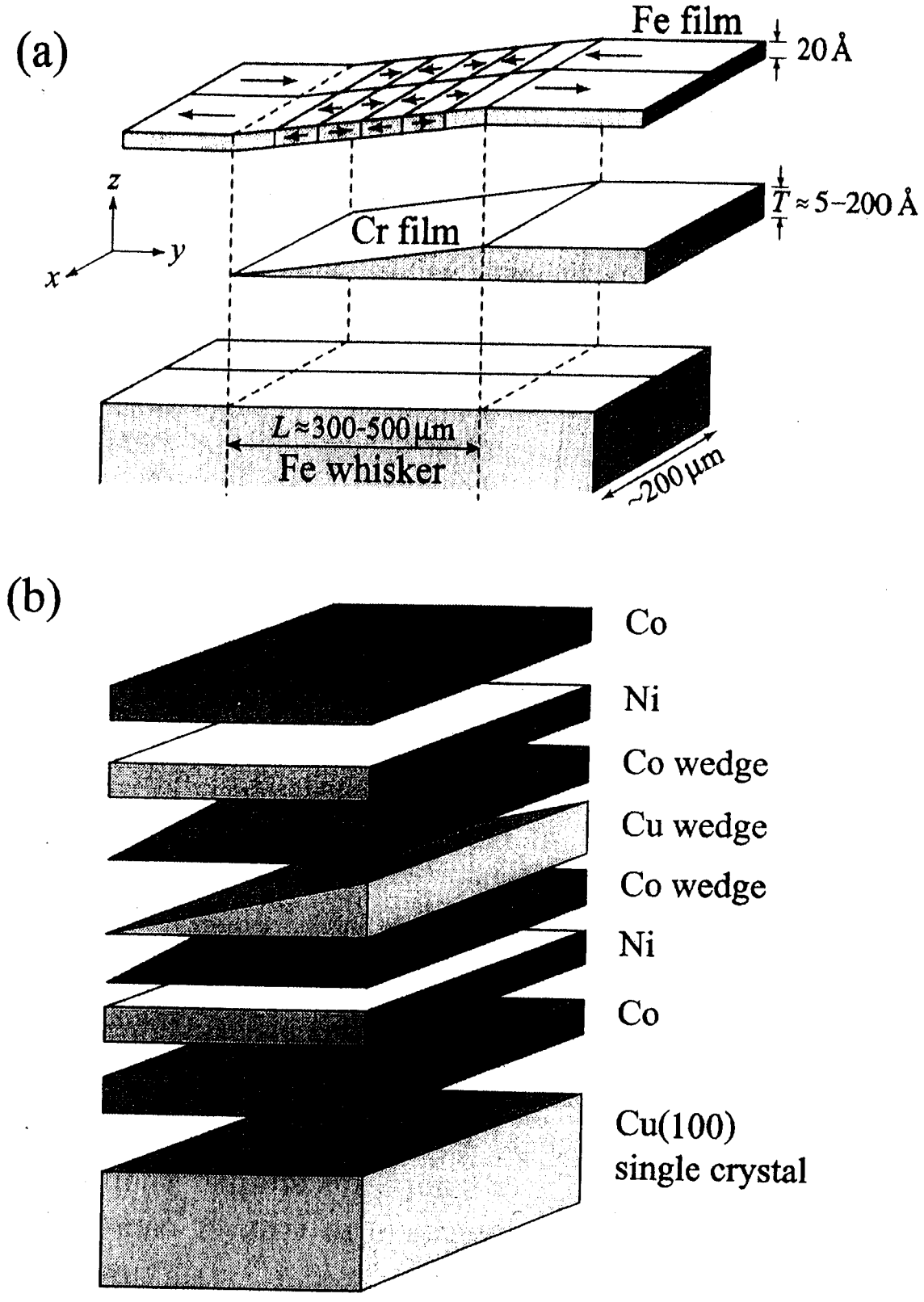

Figure 1.6: (a) simple wedge, (b) double wedges.

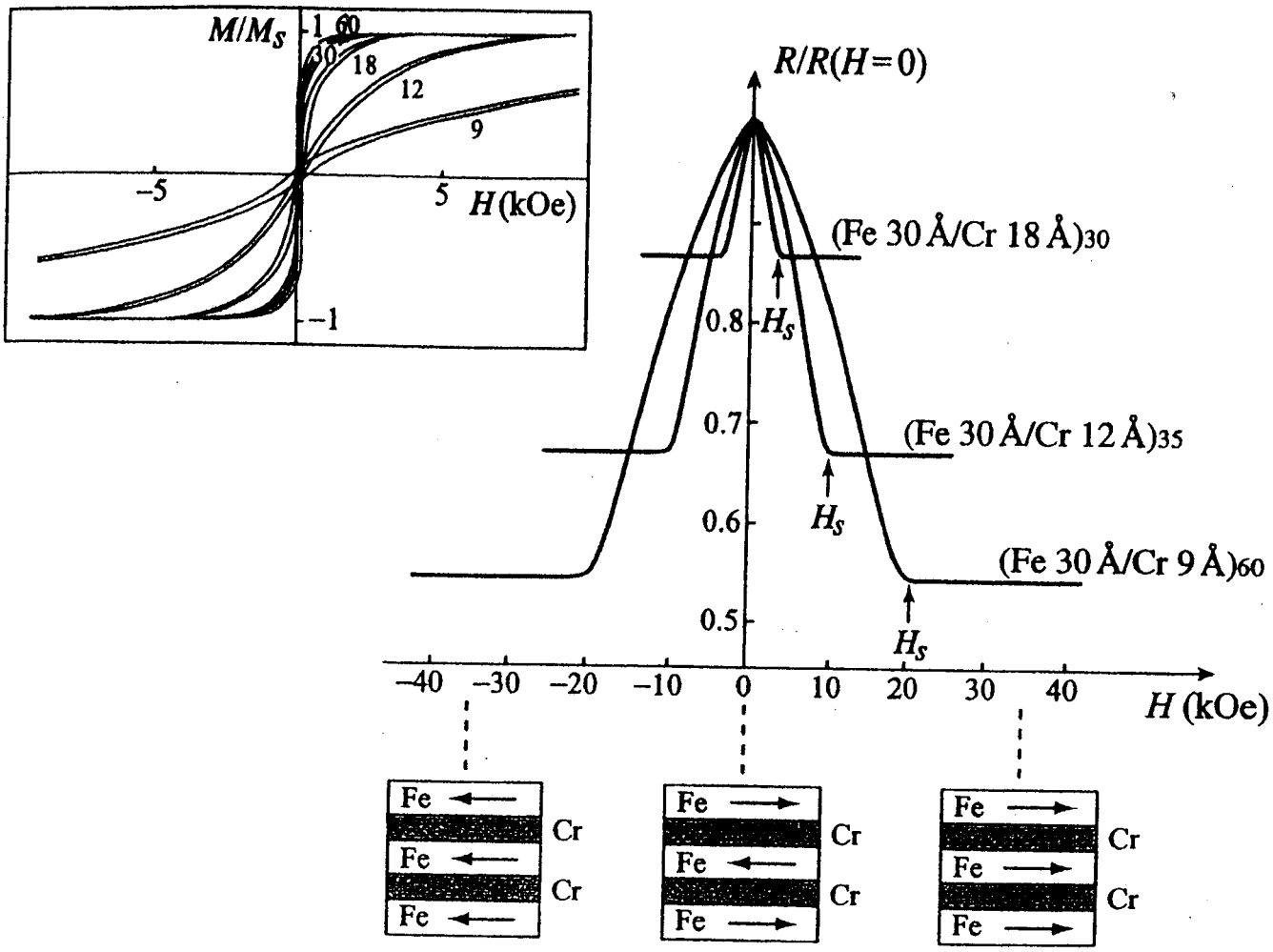

Figure 1.2: Resistivity of Fe/Cr multilayers at 4.2 K as a function of magnetic field. Magnetization curves at 4.2 K are shown in the inserted figure. The numbers represent the Cr layer thicknesses [1].

Fig 1.9

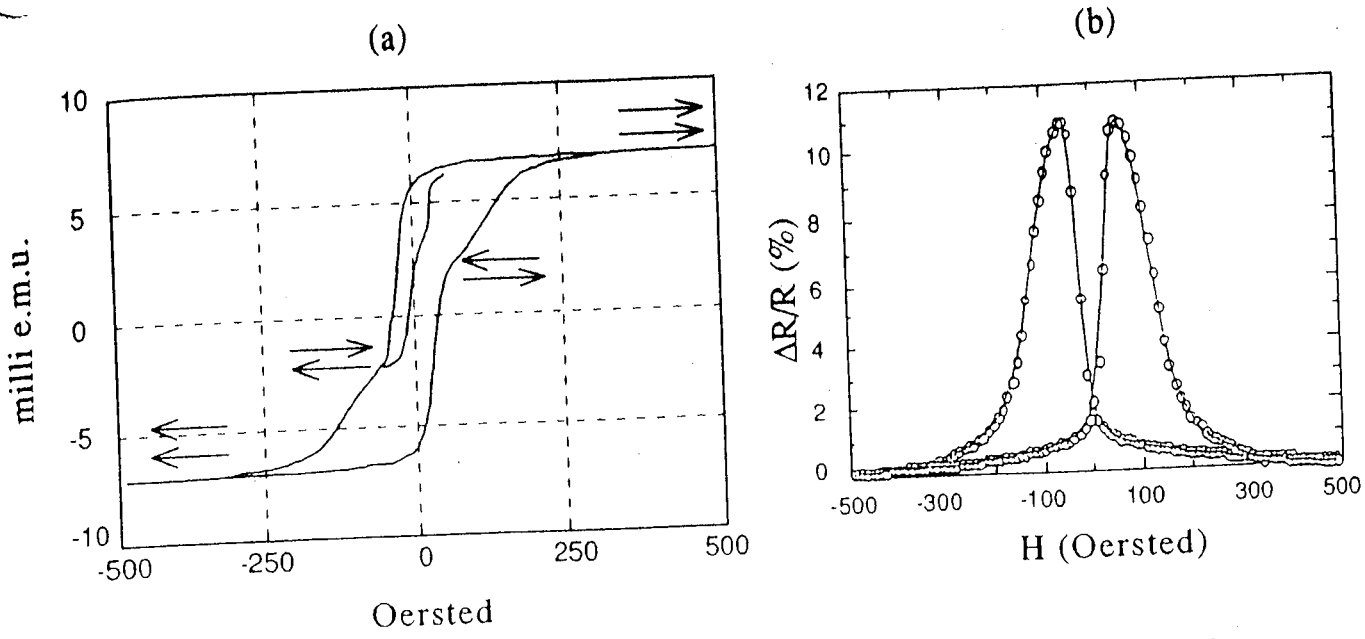

Si(100)/Fe(50 Å)/[Ni80Fe20(50 Å)/Cu(20 Å)/Co(20 Å)/Cu(20 Å)]18

Fig.27 M-H loop and magnetoresistance loop for a Si(100)/Fe(5nm) / [$Ni_{80}Fe_{20}$ (5nm)/Cu (2nm)/Co (2nm)/Cu(2nm)]×18.

Fig 17

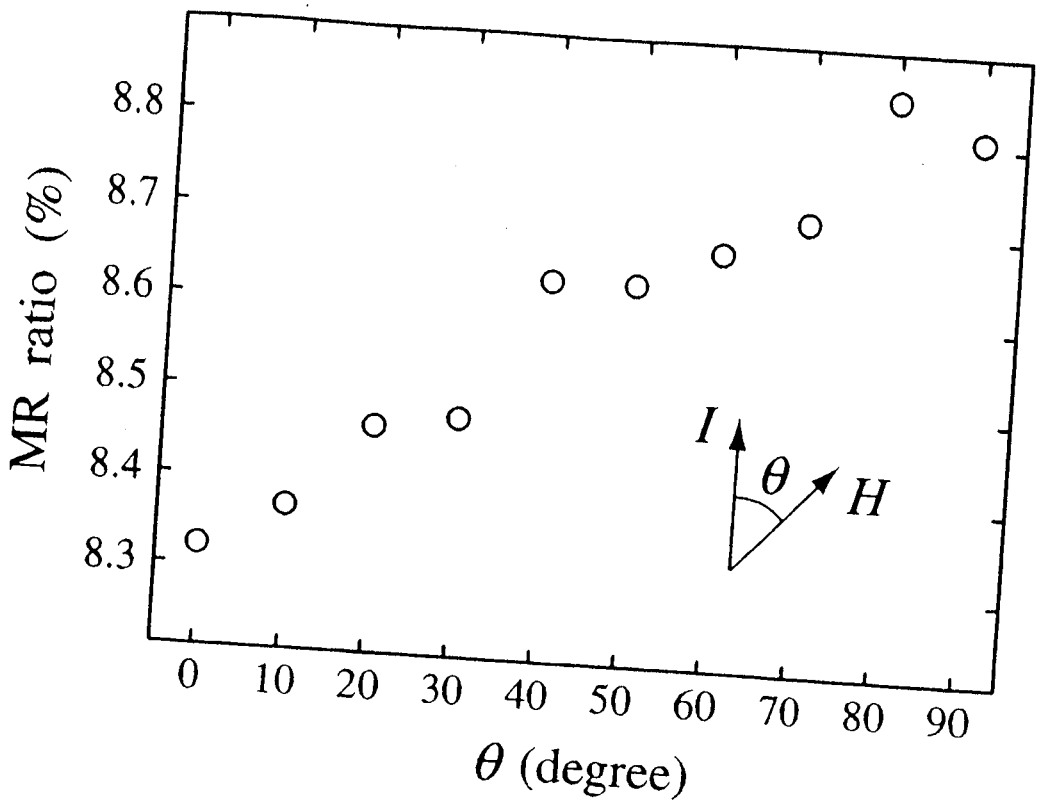

Figure 1.8: Non-coupled type GMR ratio in [NiFe 25 Å/Cu 55 Å/Co 25 Å/Cu 55 Å]×15 as a function of the angle between the magnetic field and the electric current [30].

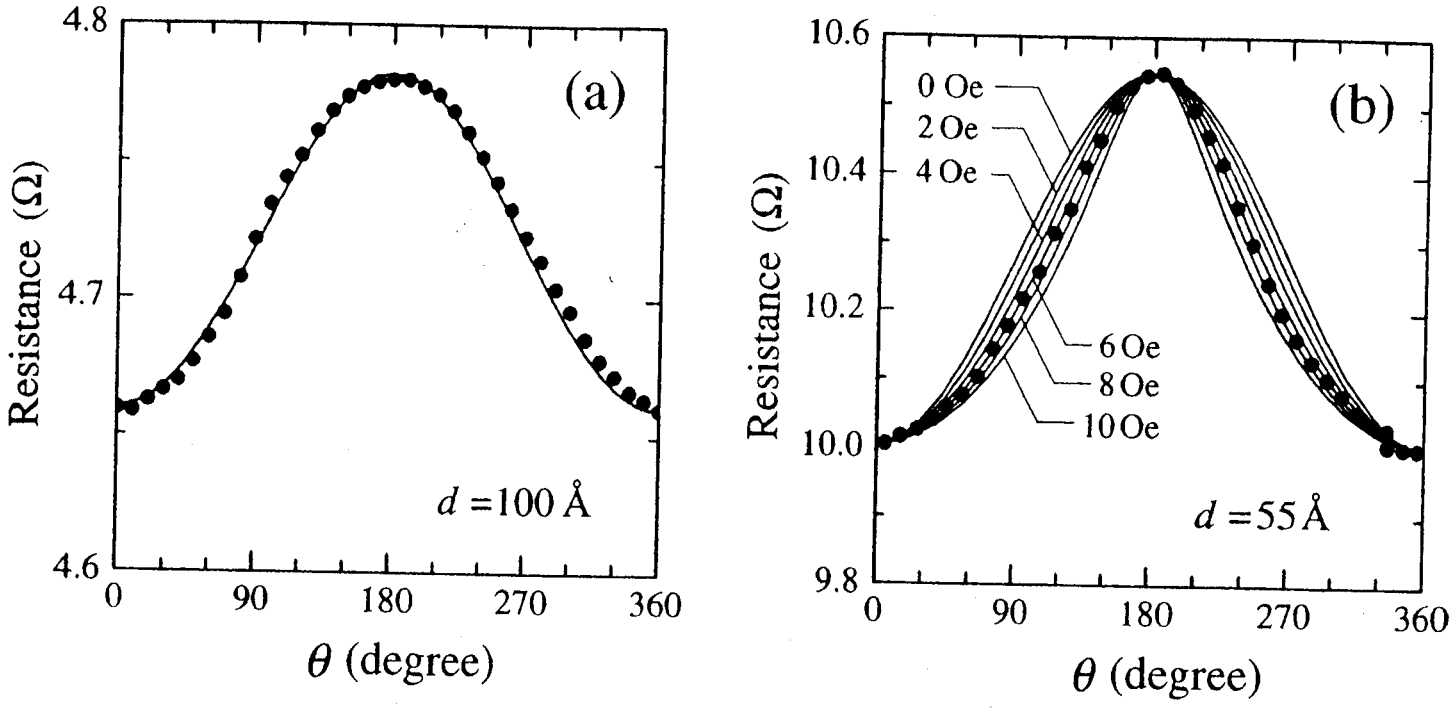

Figure 1.9: MR effect of [Cu(d)/Co 25 Å/Cu(d)/NiFe 25 Å]×15 at 300 K under a rotating field of 20 Oe. The angle θ means the direction of the external field (a) d=100 Å and (b) d = 55 Å [31].

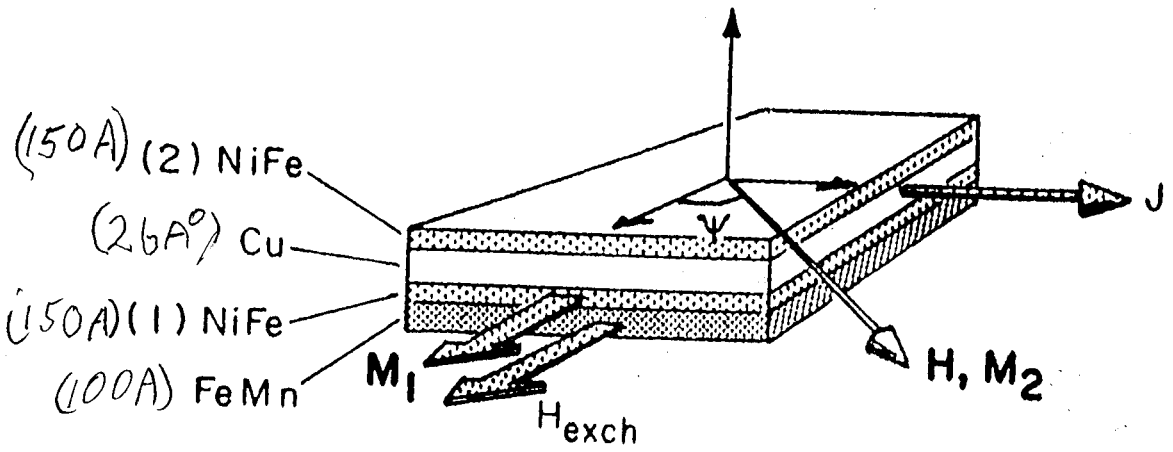

Figure 15.33 Typical composite film structure for spin valve effect. Permalloy layer (1) s exchange-coupled to the FeMn layer. Permalloy layer (2) is weakly coupled to layer 1). The magnetization of layer (2), M_2, can be arbitrarily oriented by an external field hat is too weak to significantly perturb the orientation of M_1.

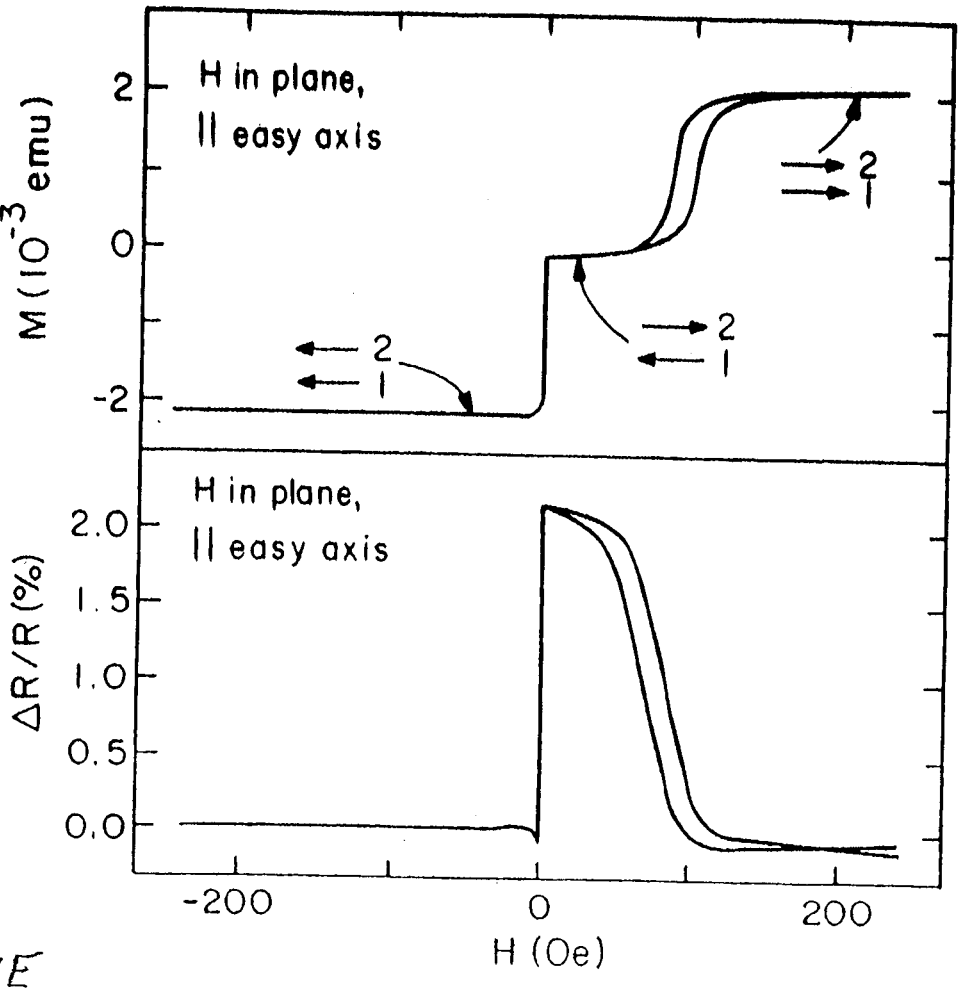

Spin VALVE

Figure 15.34 Room temperature magnetization and relative change in resistance for Si/(NiFe 150 Å)/(Cu 26 Å)/(NiFe 150 Å)/(FeMn 100 Å)/(Ag 20 Å). Current is perpendicular to the easy axis determined by the FeMn film, which is exchange-coupled to the adjacent permalloy layer. [After Dieny *et al.* (1991).]

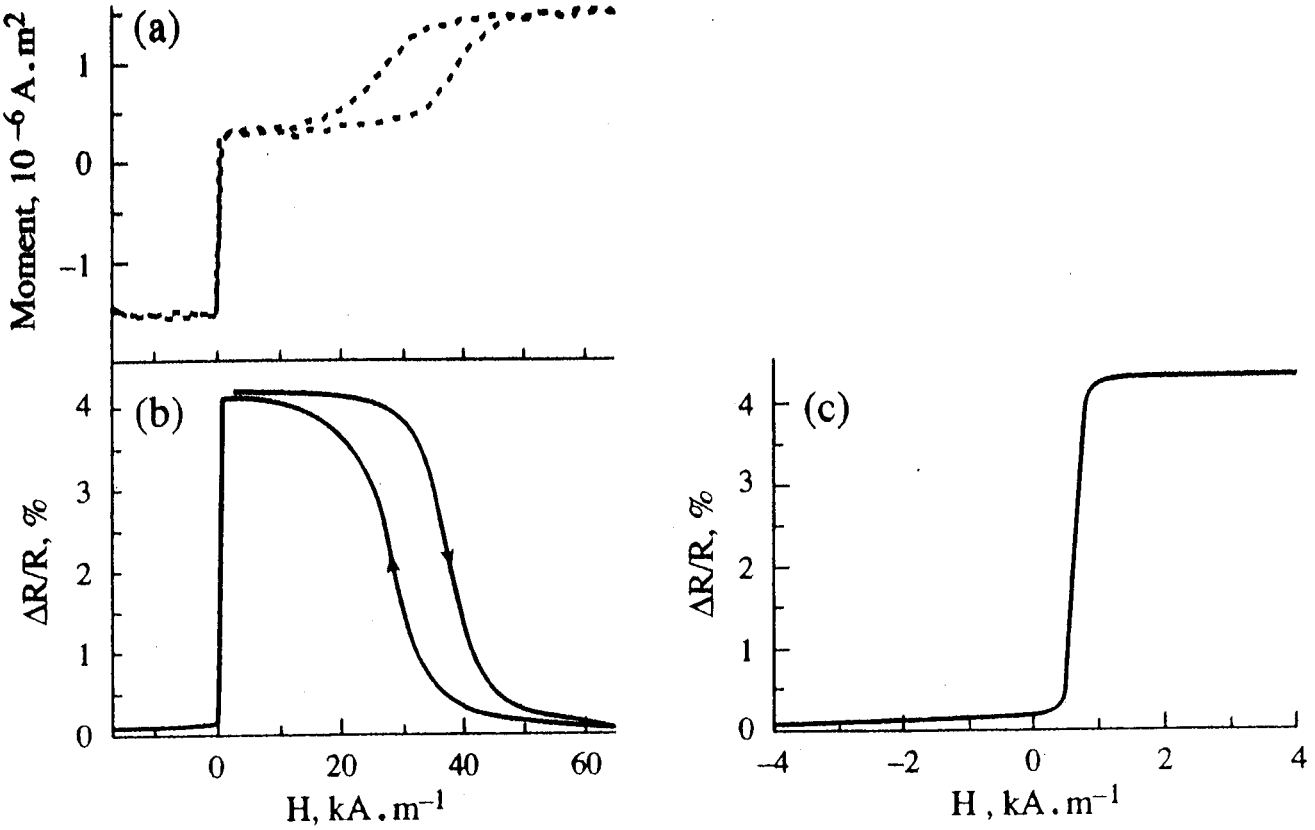

Figure 20.18 - Hysteresis loop (a) and magnetoresistance (b) at 300K of a spin valve f composition: Si/Ta 5 nm/NiFe 6 nm/Cu 2.2 nm/NiFe 4 nm/FeMn 7 nm/Ta 5 nm (c) magnetoresistance in low field [45]

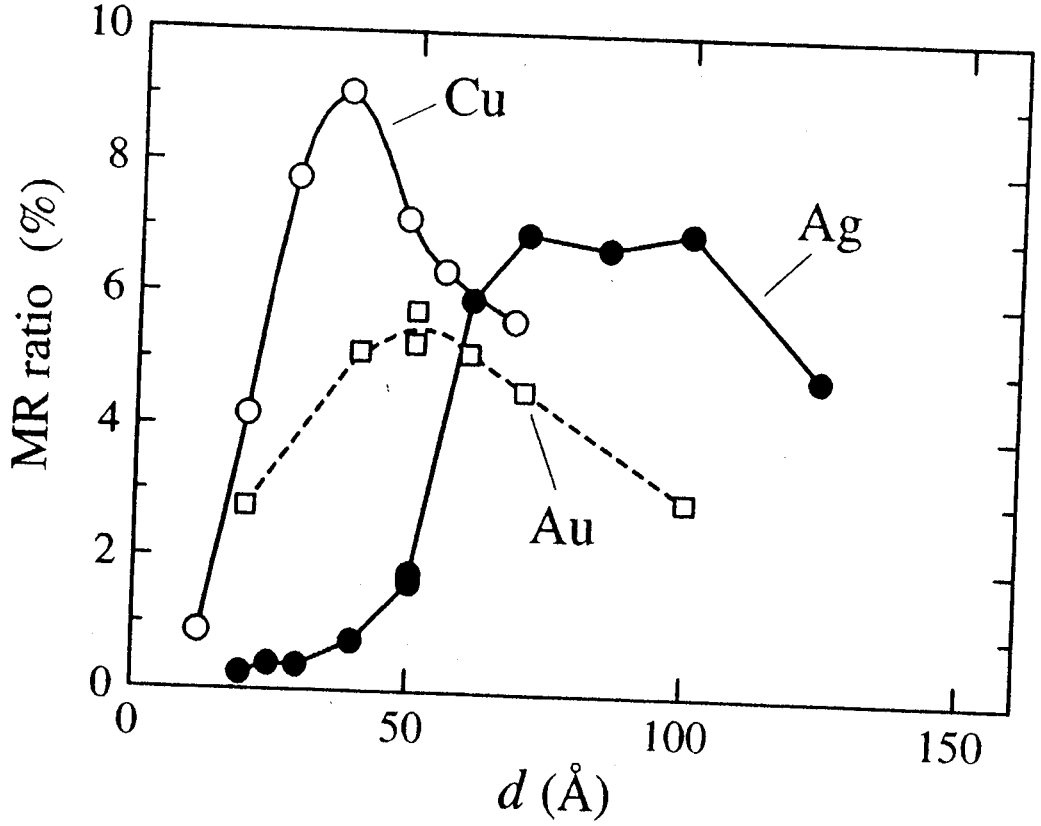

Figure 1.10: Comparison of the non-coupled type GMR effect in Cu-, Au- and Ag-based films. The thicknesses of magnetic layers (NiFe and Co) are 25 Å. number of multilayer repetition is 5, for all samples [32].

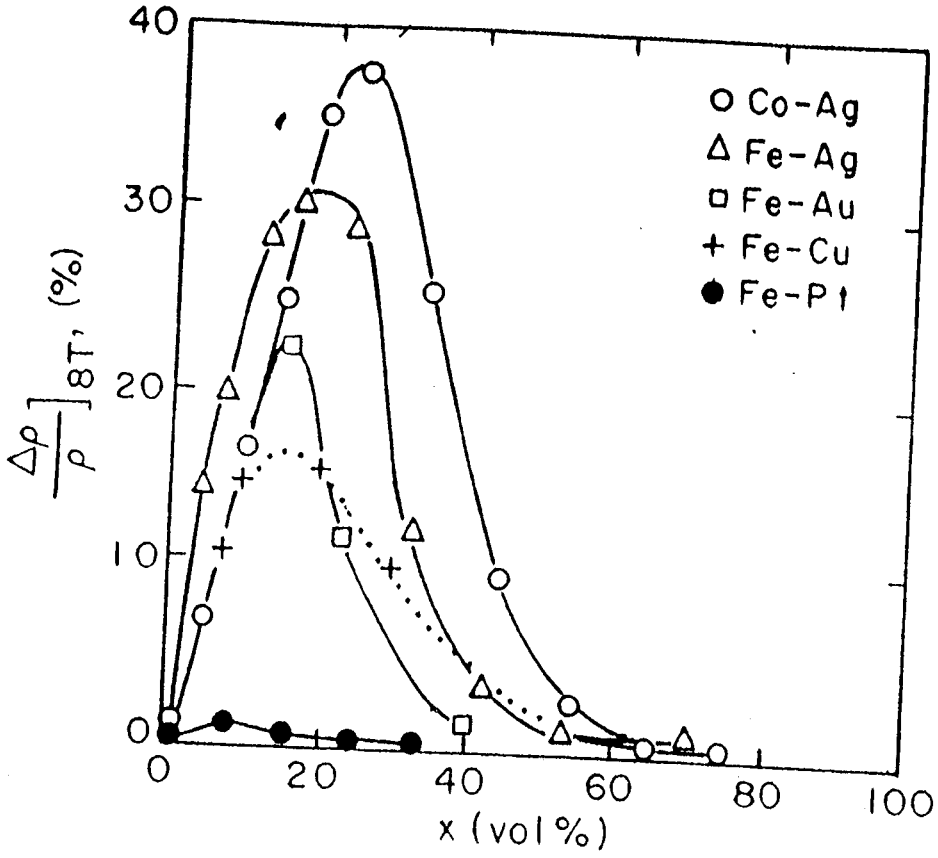

Figure 15.32 Variation of GMR at 8 T, $(\Delta\rho/\rho)_{8T}$, with volume fraction of magnetic components in several granular systems (Wang 1994).

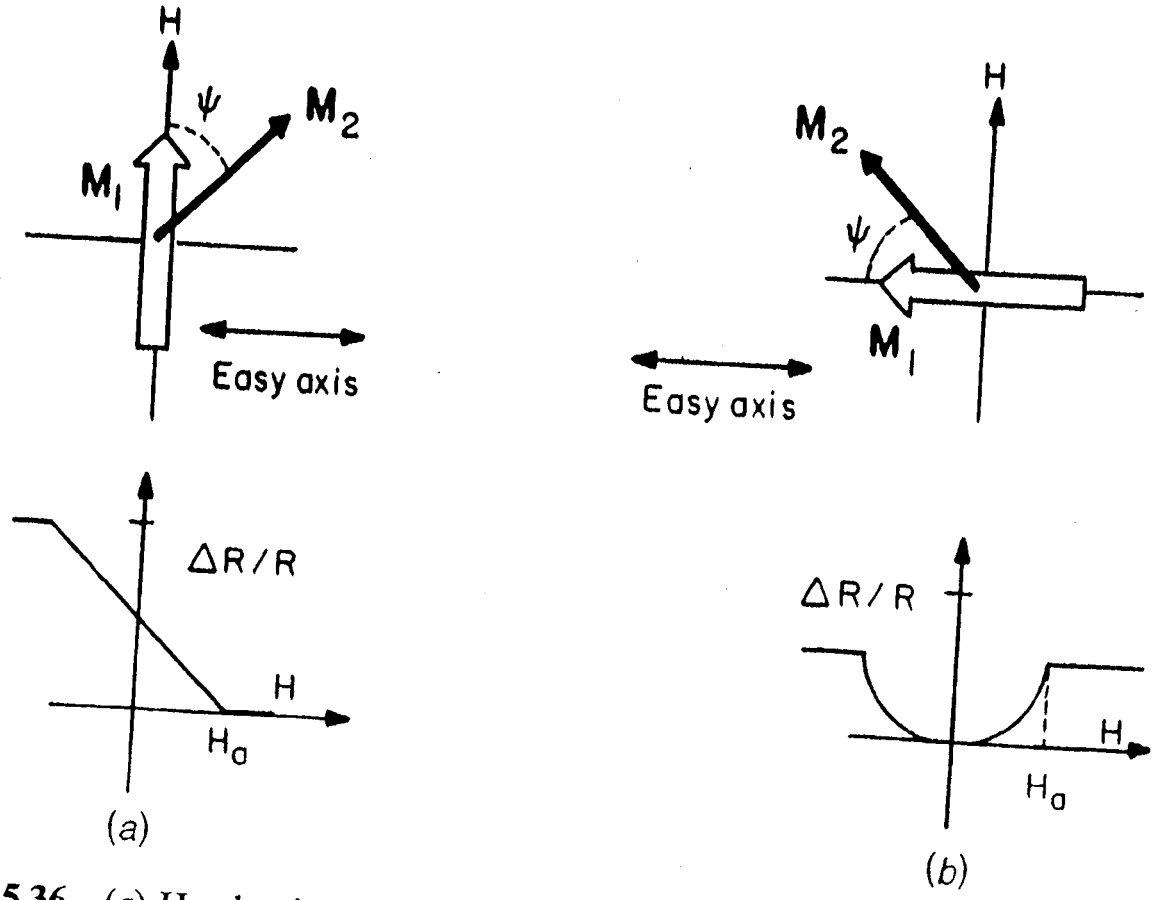

Figure 15.36 (*a*) Hard-axis magnetization process and MR for easy axis perpendicular to the reference magnetization direction (open arrow) in a spin valve structure; (*b*) hard-axis magnetization process and MR for spin valve with easy axis parallel to the reference magnetization direction.

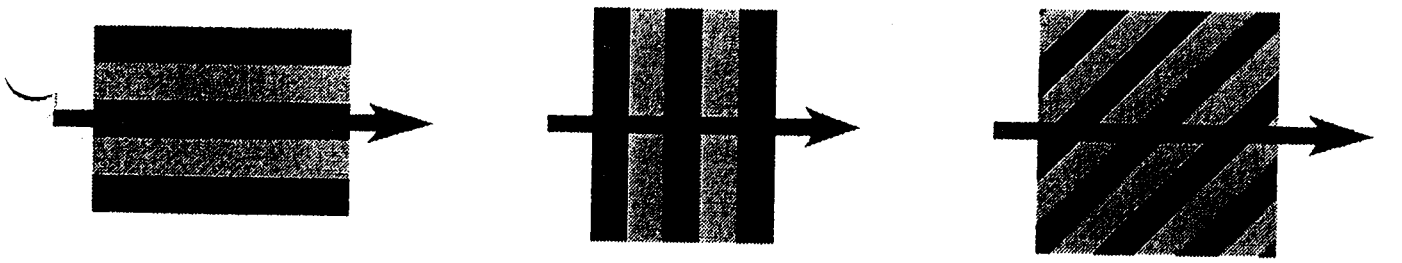

Figure 1.17: CIP, CPP, and CAP geometries.

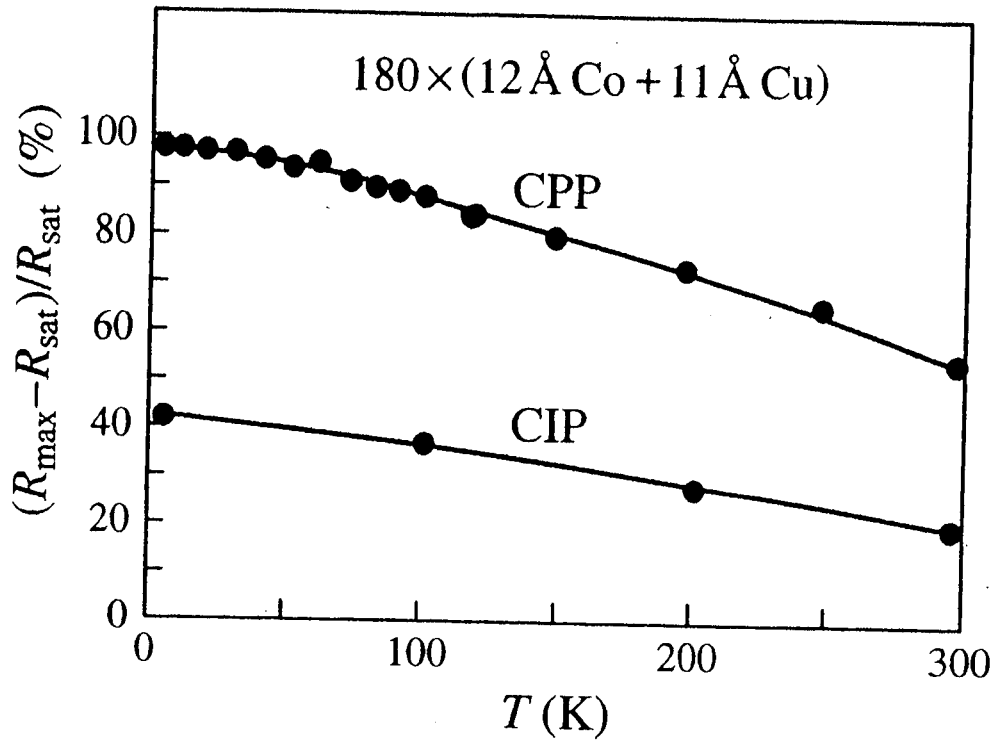

Figure 1.19: Temperature dependence of the CPP-MR of Co/Cu pillar structure [58].

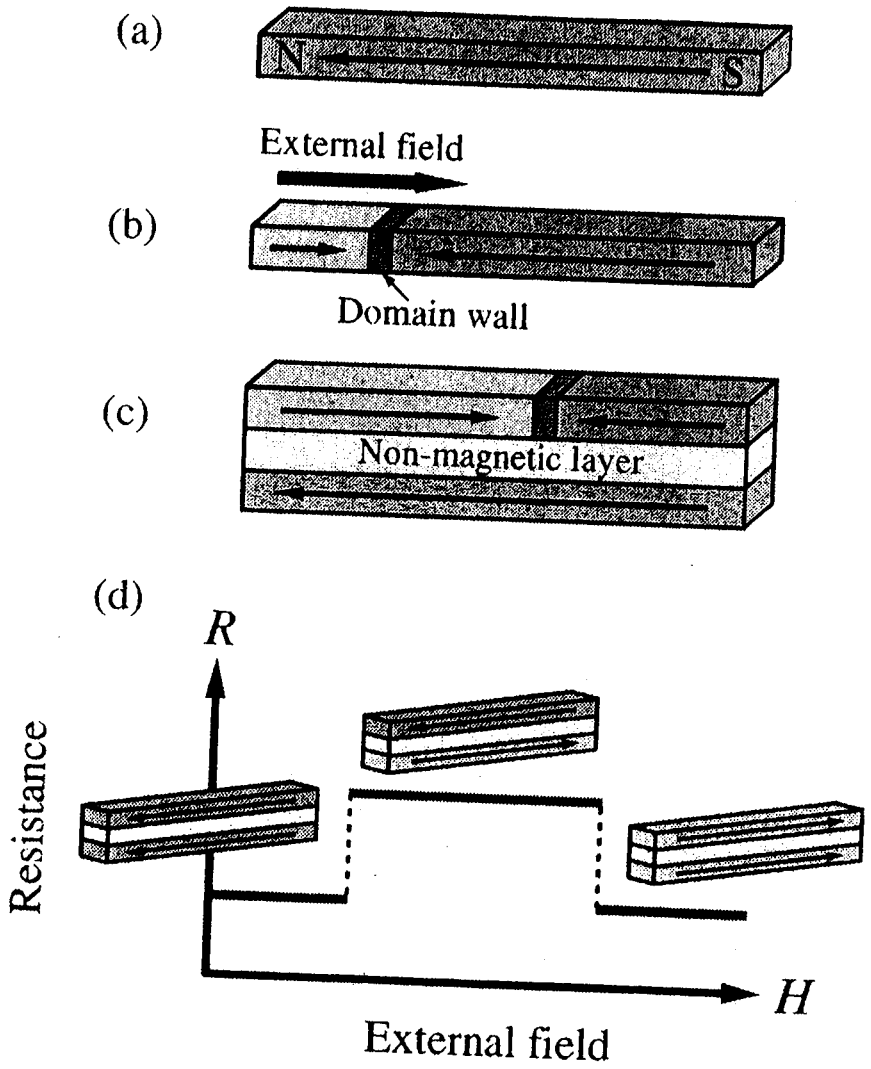

Figure 1.23: (a), (b) Magnetization reversal of a wire associating with the propagation of the domain wall. (c) Structure of trilayer system. (d) Resistance change associating with magnetization reversal.

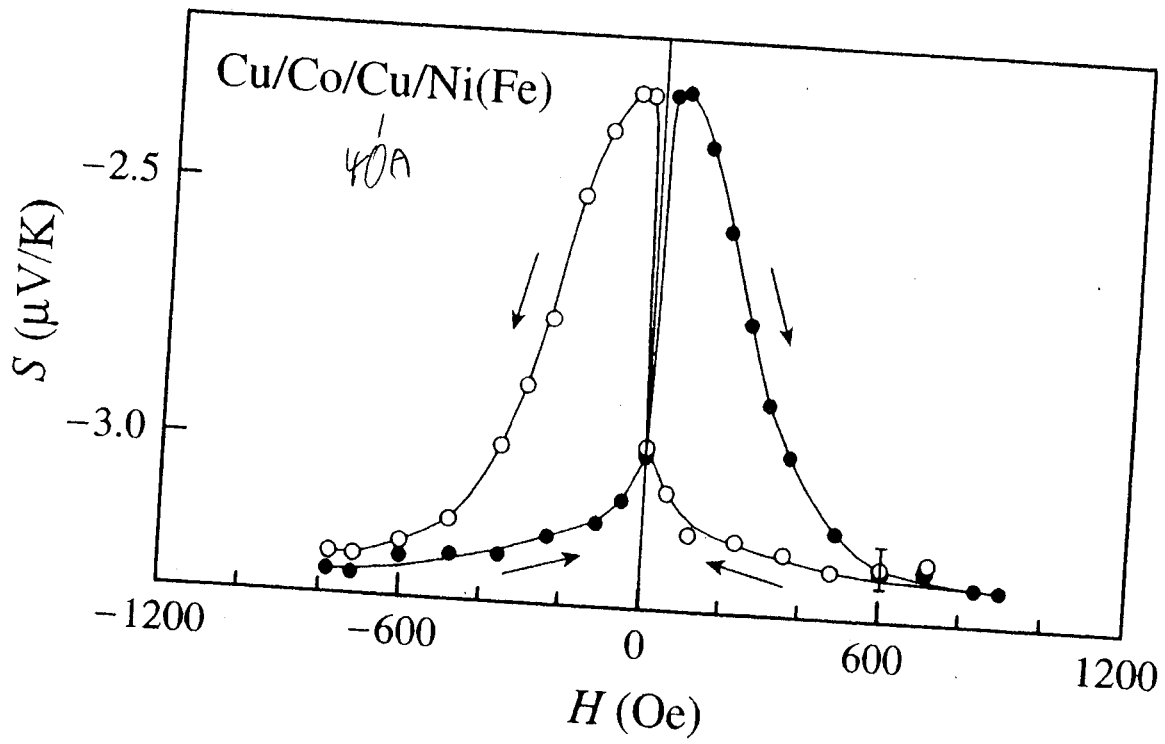

Figure 1.14: Thermopower at 80 K of Cu/Co/Cu/NiFe as a function of mag
netic field [35]. NON-COUPLED.

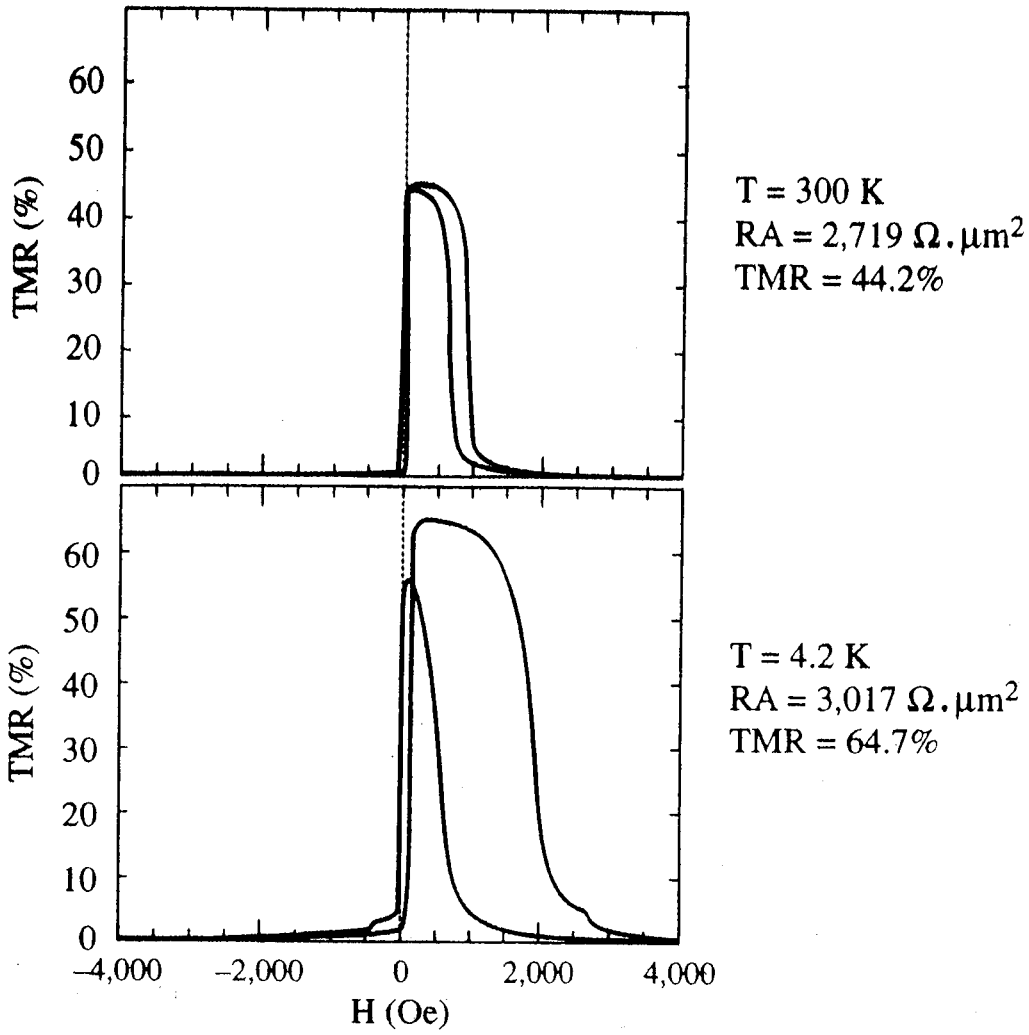

Figure 20.19 - Magnetoresistance of a tunnel junction of composition : Buffer / IrMn 10nm / CoFe 4nm / Al 0.8nm-oxide / CoFe 4nm / NiFe 20nm / Ta 5nm at room temperature and liquid helium temperature

The junction area is 5 ×5 μm^2 [after 61].